EM-Aided AMP for Sparse Channel Recovery and Ranging in Nakagami-m Fading

Xiyao Zhou, Fangqing Xiao, and Dirk Slock
EURECOM, Sophia Antipolis, France
Email: {xiyao.zhou, fangqing.xiao, dirk.slock}@eurecom.fr

***Abstract*—Accurate recovery of sparse channels and line-of-sight (LoS) distances is essential for integrated sensing and communications (ISAC). Conventional approximate message passing (AMP) approaches typically adopt Gaussian or Bernoulli–Gaussian priors, which fail to capture realistic fading and lead to biased amplitude estimates. We propose an Expectation–Maximization aided AMP (EM–AMP) framework tailored to the Nakagami-m prior. A closed-form denoiser is derived and embedded in the EM loop, enabling the average path power to be learned directly from data. On top of this, a hybrid estimator combines AMP-based probabilistic support detection with a least-squares refit, mitigating shrinkage bias and sharpening power–delay profiles for robust ranging. Monte Carlo simulations show that while greedy algorithms like OMP achieve low residual channel errors, they suffer from severe amplitude bias and missed paths under Nakagami-m fading. The proposed EM-AMP framework improves support recall and reduces the ranging mean-squared error (MSE) by approximately 3 dB at high SNRs, making it highly robust for practical ISAC deployments.**

***Index Terms*—Approximate Message Passing, Sparse Channel Estimation, Nakagami-m Fading, Integrated Sensing and Communications, Expectation–Maximization**

I. Introduction

Integrated sensing and communications (ISAC) reuses resources so a single platform provides both data connectivity and environment perception [1]. In many OFDM-style receivers, the effective sensing operator is circulant or partial-Fourier, and the delay-domain channel is naturally sparse: only a few resolvable taps carry most of the energy. Recovering this sparse multipath structure is therefore essential not only for reliable demodulation but also for geometry extraction tasks such as line-of-sight (LoS) ranging from the power–delay profile (PDP), as emphasized in recent ISAC surveys [2].

We adopt the standard pilot–observation setting widely used in OFDM channel estimation [3]. Each active tap has a uniformly random phase and a propagation-dependent amplitude. Among fading models, the Nakagami-m family offers a flexible description that spans rich scattering to near-LoS conditions and subsumes Rayleigh and Rician behaviors [4], [5]. In practice, key fading parameters such as the average path power vary with the environment and are typically unknown. Identifiability is ensured by standard pilot- and column-energy normalizations. We focus on quasi-static channels without explicit Doppler, consistent with many ISAC snapshots [1], and later connect recovered amplitudes to a path-loss model for ranging [6].

Classical sparse recovery methods such as OMP and LASSO provide fast baselines but are highly sensitive to off-grid delays and basis mismatch, which smear PDP peaks and bias amplitudes [7]–[9]. Approximate Message Passing (AMP) is more attractive in ISAC since it exploits FFT-structured operators and admits rigorous large-system analysis via state evolution [10]–[13]. However, most AMP deployments assume Gaussian-type priors for convenience. Under realistic fading, these mismatched priors cause systematic *shrinkage* of tap magnitudes—supports may appear correct, but amplitudes are underestimated, directly degrading ranging accuracy. Type-II/SBL and VAMP alleviate prior mismatch but incur higher per-iteration cost or require heavy factorizations, making them less suitable for low-latency ISAC [13]–[15].

Because fading statistics vary across environments, adaptive parameter learning is necessary. Expectation–Maximization (EM) provides a principled mechanism to infer unknown statistical parameters while treating the sparse channel as latent [16]. Each EM cycle alternates between approximate posterior inference and parameter updates, enabling adaptation to scene-dependent fading without hand tuning.

Exact posterior inference is infeasible at ISAC scales. AMP offers an efficient approximation for the E-step, with FFT-level complexity and state-evolution diagnostics to guide convergence [10]–[13]. Prior EM-within-AMP designs have focused on Gaussian or Bernoulli–Gaussian priors and on learning parameters such as noise variance or sparsity rates [17], but remain vulnerable when real fading amplitudes deviate from these simplistic assumptions.

In this work, we propose a model-driven EM–AMP pipeline tailored to Nakagami-m amplitude statistics. The shape parameter is fixed, while the average path power is learned adaptively through log-domain EM updates, combining physical realism with numerical stability. To mitigate AMP shrinkage before geometry extraction, we augment the inference with a lightweight least-squares refit on the AMP-selected support [18], which sharpens PDP peaks and improves ranging. Finally, LoS distance is estimated via a one-dimensional likelihood search based on the path-loss law [6]. The overall framework remains FFT-efficient and compatible with ISAC latency requirements.

II. System and Signal Model

We focus on quasi-static channels to establish the core sparse recovery framework; the integration of Doppler compensation for high-mobility ISAC scenarios is deferred to future work.

We consider pilot-aided recovery of sparse wideband channels and ranging in OFDM systems [19]. The formulation proceeds from the time-domain observation model, through the FFT-structured sensing matrix, to the statistical prior and path-loss parameterization that links the channel to geometry.

A. Time-Domain Observation Model

After cyclic prefix (CP) removal, consider one OFDM/SC block with N samples and sampling period T_s. For an L-path channel with complex gains $\{\alpha_\ell\}$ and integer-sample delays $\tau_\ell = q_\ell T_s$ ($q_\ell \in \{0, \dots, N-1\}$, ignoring Doppler), the received block is [20]:

$$y[n] = \sum_{\ell=1}^{L} \alpha_\ell \sum_{k=0}^{N-1} \mathrm{sinc}_N(n - k - q_\ell)\, s[k] + v[n], \qquad n = 0, \dots, N-1, \tag{1}$$

where $\mathbf{s} \in \mathbb{C}^N$ is the known pilot (QPSK, $\|\mathbf{s}\|_2^2 = N$), and $v[n]$ is additive white noise. The periodic discrete-time sinc (Dirichlet kernel) is

$$\mathrm{sinc}_N(u) \;= \frac{1}{N}\sum_{k=0}^{N-1} e^{\mathrm{j}\frac{2\pi k}{N}u} = e^{\mathrm{j}\pi\frac{N-1}{N}u}\frac{\sin(\pi u)}{N\sin(\pi u/N)}, \tag{2}$$

continued by continuity at integer u.

In matrix form,

$$\mathbf{y} = \mathbf{H}\mathbf{s} + \mathbf{v}, \qquad \mathbf{H} = \sum_{\ell=1}^{L} \alpha_\ell\, \mathbf{C}(\tau_\ell), \tag{3}$$

where the $N \times N$ circulant delay operator is

$$[\mathbf{C}(\tau)]_{n,k} = \mathrm{sinc}_N\Big(n - k - \tfrac{\tau}{T_s}\Big). \tag{4}$$

If $\tau = qT_s$ with integer q, then $\mathbf{C}(\tau)$ reduces to a q-sample circular shift.

B. On-Grid Dictionary Formulation

To cast the problem as sparse recovery, we form the delay dictionary

$$\mathbf{A} = \big[\mathbf{a}_0, \mathbf{a}_1, \ldots, \mathbf{a}_{N-1}\big], \quad \mathbf{a}_n = \mathbf{C}(nT_s)\mathbf{s}, \tag{5}$$

and collect effective tap gains into a sparse vector $\mathbf{x} \in \mathbb{C}^N$. The resulting linear model is

$$\mathbf{y} = \mathbf{A}\mathbf{x} + \mathbf{v}, \tag{6}$$

which serves as the basis for subsequent inference. For integer delays, each path aligns with one column of $\mathbf{A}$ without leakage. Each column is normalized to unit ℓ_2 norm:

$$\mathbf{a}_n \leftarrow \mathbf{a}_n/\|\mathbf{a}_n\|_2, \qquad n = 0, \ldots, N-1. \tag{7}$$

This dictionary structure preserves FFT efficiency $\mathcal{O}(N\log N)$ and coincides with the circulant model under on-grid delays.

C. Bernoulli–Nakagami-m Prior

Let $\mathcal{S} \subset \{1, \ldots, N\}$ be the active support with $|\mathcal{S}| = k$. For $n \notin \mathcal{S}$, $x_n = 0$; for $n \in \mathcal{S}$, write $x_n = \rho_n e^{\mathrm{j}\phi_n}$ with $\phi_n \sim \mathrm{Unif}[0, 2\pi)$ and $\rho_n \sim$ Nakagami-$m(\Omega_n)$:

$$f_{\rho_n}(\rho) = \frac{2m^m}{\Gamma(m)\Omega_n^m}\,\rho^{2m-1}\exp\Big(-\tfrac{m}{\Omega_n}\rho^2\Big), \quad \rho > 0. \tag{8}$$

The induced complex slab density is

$$p_{\mathrm{slab}}(x_n \mid m, \Omega_n) = \frac{m^m}{\pi\,\Gamma(m)\Omega_n^m}\,|x_n|^{2m-2}\exp\Big(-\tfrac{m}{\Omega_n}|x_n|^2\Big). \tag{9}$$

Thus the spike-and-slab prior is

$$p(x_n \mid \rho, m, \Omega_n) = (1-\rho)\,\delta(x_n) + \rho\, p_{\mathrm{slab}}(x_n \mid m, \Omega_n). \tag{10}$$

This prior captures both sparsity and realistic fading; the shape parameter m controls tail behavior.

D. Path-Loss Power and Ranging Parameter

To link channel statistics with geometry, the average power of tap n is modeled as [21]:

$$\Omega_n(d_0) = G\,(d_0 + n\,\Delta d)^{-\gamma}, \qquad n = 0, \ldots, N-1, \tag{11}$$

where $G > 0$ is a path-gain constant, $\Delta d > 0$ is the delay-bin resolution, $\gamma > 0$ is the path-loss exponent, and $d_0 > 0$ is the unknown LoS distance. Early taps dominate under this law, providing ranging information. Deviations from the ideal profile are absorbed by the slab prior and noise. Here d_0 is introduced for the first time as the key geometry parameter to be estimated jointly with $\mathbf{x}$.

E. Noise and Identifiability

Noise is spatially white with variance σ_v^2. Column normalization and pilot normalization fix the global scale, preventing confounding between (σ_v^2, Ω_n) and $\|\mathbf{A}\|$. The complete parameter set is

$$\Theta = \{\rho,\, m,\, d_0,\, \{\Omega_n(d_0)\}_n,\, \sigma_v^2\}, \tag{12}$$

with m treated as known in the baseline. Equations (6)–(10) and the path-loss model define a structured linear inverse problem with a physically informed sparse prior. This model sets the stage for the EM–AMP inference described in the next section.

III. Proposed EM-Aided AMP Framework

Building on the structured model in Sec. II, we now describe an inference framework that integrates Approximate Message Passing (AMP) with Expectation–Maximization (EM). AMP provides efficient approximate posterior moments under the scalar effective channels, corresponding to the E-step of EM, while the M-step updates prior parameters using these moments. After convergence, a final maximum-likelihood stage estimates the physical LoS distance d_0 and the per-tap powers $\{\Omega_n(d_0)\}$.

A. AMP with a Bernoulli–Nakagami-m Denoiser

Given the linear inverse model in (6), AMP decouples high-dimensional inference into scalar denoising problems. To achieve this, at each iteration t, a Gaussian pseudo-observation vector $\mathbf{r}^{(t)}$ is formed by combining the current estimate with the matched-filtered residual:

$$\mathbf{r}^{(t)} = \hat{\mathbf{x}}^{(t)} + \mathbf{A}^{\mathrm{H}}\mathbf{z}^{(t)}, \tag{13}$$

$$\tau_r^{(t)} = \tfrac{1}{N}\,\|\mathbf{z}^{(t)}\|_2^2, \tag{14}$$

where $\tau_r^{(t)}$ represents the variance of the effective additive white Gaussian noise (AWGN) in the pseudo-observation model, which is estimated from the power of the residual vector $\mathbf{z}^{(t)}$. Under the large-system limit, each coordinate approximately follows a scalar Gaussian channel: $r_n^{(t)} \sim \mathcal{CN}(x_n,\, \tau_r^{(t)})$. With the Bernoulli–Nakagami-m prior in (10), the denoiser $\eta(\cdot)$ computes the approximate posterior mean and variance:

$$\hat{x}_n^{(t+1)} = \mathbb{E}[x_n \mid r_n^{(t)}, \tau_r^{(t)}; m, \Omega^{(t)}] = \pi_n^{(t)}\,\hat{x}_{n,\mathrm{slab}}^{(t+1)}, \tag{15}$$

$$v_n^{(t+1)} = \mathrm{Var}[x_n \mid r_n^{(t)}, \tau_r^{(t)}; m, \Omega^{(t)}], \tag{16}$$

where $\pi_n^{(t)}$ is the posterior activity probability and $\hat{x}_{n,\mathrm{slab}}^{(t+1)}$ denotes the slab-conditional mean estimate.

a) Onsager correction.: The AMP residual update is

$$\mathbf{z}^{(t+1)} = \mathbf{y} - \mathbf{A}\hat{\mathbf{x}}^{(t+1)} + \mathbf{z}^{(t)}\,\big\langle \eta' \big\rangle^{(t+1)}, \tag{17}$$

with divergence approximation

$$\big\langle \eta' \big\rangle^{(t+1)} \approx \tfrac{1}{N}\sum_{n=1}^{N} \tfrac{v_n^{(t+1)}}{\tau_r^{(t)}}. \tag{18}$$

b) Damping.: To stabilize iterations, we apply damping with factor $\beta \in (0, 1]$:

$$\tilde{\mathbf{x}}^{(t+1)} = \eta(\mathbf{r}^{(t)}, \tau_r^{(t)}; m, \Omega^{(t)}), \tag{19}$$

$$\tilde{\mathbf{z}}^{(t+1)} = \mathbf{y} - \mathbf{A}\tilde{\mathbf{x}}^{(t+1)} + \mathbf{z}^{(t)}\,\big\langle \eta' \big\rangle^{(t+1)}, \tag{20}$$

$$\mathbf{x}^{(t+1)} = (1-\boldsymbol{\beta})\,\mathbf{x}^{(t)} + \boldsymbol{\beta}\,\tilde{\mathbf{x}}^{(t+1)}, \tag{21}$$

$$\mathbf{z}^{(t+1)} = (1-\boldsymbol{\beta})\,\mathbf{z}^{(t)} + \boldsymbol{\beta}\,\tilde{\mathbf{z}}^{(t+1)}, \tag{22}$$

$$\tau_r^{(t)} = \tfrac{1}{N}\,\|\mathbf{z}^{(t)}\|_2^2. \tag{23}$$

c) Closed-form Nakagami-m posterior.: Define

$$\zeta_n^{(t)} \triangleq \frac{\Omega^{(t)}|r_n^{(t)}|^2}{m(\tau_r^{(t)})^2 + \tau_r^{(t)}\Omega^{(t)}}. \tag{24}$$

For the joint density $\mathcal{CN}(r_n^{(t)}; x_n, \tau_r^{(t)})\, p_{\mathrm{slab}}(x_n \mid m, \Omega^{(t)})$, the slab-conditional moments are [5]

$$\hat{x}_{n,\mathrm{slab}}^{(t+1)} = \frac{m\Omega^{(t)} r_n^{(t)}}{m\tau_r^{(t)} + \Omega^{(t)}} \frac{{}_1F_1(m{+}1;\, 2;\, \zeta_n^{(t)})}{{}_1F_1(m;\, 1;\, \zeta_n^{(t)})}, \tag{25}$$

$$\mathbb{E}[|x_n|^2 \mid \mathrm{slab}]^{(t+1)} = \frac{m\Omega^{(t)} \tau_r^{(t)}}{m\tau_r^{(t)} + \Omega^{(t)}} \frac{{}_1F_1(m{+}1;\, 1;\, \zeta_n^{(t)})}{{}_1F_1(m;\, 1;\, \zeta_n^{(t)})}, \tag{26}$$

$$\tau_n^{\mathrm{slab}\,(t+1)} = \mathbb{E}[|x_n|^2 \mid \mathrm{slab}]^{(t+1)} - \big|\hat{x}_{n,\mathrm{slab}}^{(t+1)}\big|^2. \tag{27}$$

d) Spike–and–slab mixing.: Finally,

$$\hat{x}_n^{(t+1)} = \pi_n^{(t)}\, \hat{x}_{n,\mathrm{slab}}^{(t+1)}, \tag{28}$$

$$v_n^{(t+1)} = \pi_n^{(t)}\, \mathbb{E}[|x_n|^2 \mid \mathrm{slab}]^{(t+1)} - \big|\hat{x}_n^{(t+1)}\big|^2. \tag{29}$$

B. EM-Based Hyperparameter Learning

To ensure stability, EM-AMP uses a uniform power Ω during iterations, avoiding the non-convexity of joint d_0 estimation. After support identification, d_0 is extracted via the rigorous model $\Omega_n(d_0)$ and refined LS (Sec. III-C).

The average slab power Ω is learned by EM, using the posterior moments already produced by AMP. One outer EM iteration consists of:

a) E-step.: From Sec. III-A, AMP yields $\hat{x}_i^{(t+1)}$, $v_i^{(t+1)}$, and $\pi_i^{(t)}$. The per-coordinate second moment is

$$m_{2,i}^{(t+1)} \triangleq \mathbb{E}[|x_i|^2 \mid \mathbf{y}] = v_i^{(t+1)} + \big|\hat{x}_i^{(t+1)}\big|^2. \tag{30}$$

b) M-step.: Since $\log p(\mathbf{y} \mid \mathbf{x})$ does not depend on Ω, the update maximizes the expected log-prior:

$$\Omega_{\mathrm{EM}}^{(t+1)} = \frac{\sum_{i=1}^N \pi_i^{(t)}\, m_{2,i}^{(t+1)}}{\sum_{i=1}^N \pi_i^{(t)}}. \tag{31}$$

To improve robustness under uncertain support, we adopt a generalized-EM (GEM) update. Let $\mathcal{I}$ be the top-k indices of $\pi_i^{(t)}$; compute a ridge LS proxy:

$$\widehat{\mathbf{x}}_{\mathrm{LS},\mathcal{I}} = \left(\mathbf{A}_{\mathcal{I}}^{\mathrm{H}}\mathbf{A}_{\mathcal{I}} + \lambda\mathbf{I}\right)^{-1}\mathbf{A}_{\mathcal{I}}^{\mathrm{H}}\mathbf{y}, \qquad \lambda \geq 0. \tag{32}$$

Form the estimates

$$\widehat{\Omega}_{\mathrm{LS}} = \tfrac{1}{|\mathcal{I}|}\sum_{i\in\mathcal{I}} |\widehat{x}_{\mathrm{LS},i}|^2, \qquad \widehat{\Omega}_{\mathrm{mom}} = \tfrac{1}{|\mathcal{I}|}\sum_{i\in\mathcal{I}} m_{2,i}^{(t+1)}. \tag{33}$$

The damped blend is

$$\Omega^{(t+1)} = (1-\alpha_\Omega)\,\Omega^{(t)} + \alpha_\Omega\Big(\omega\,\widehat{\Omega}_{\mathrm{LS}} + (1-\omega)\,\widehat{\Omega}_{\mathrm{mom}}\Big), \tag{34}$$

with $\alpha_\Omega \in (0,1]$ and $\omega \in [0,1]$.

For stability and reproducibility, hyperparameters are empirically set to: damping $\beta = 0.3$, ridge parameter $\lambda = 10^{-3}$ (for invertibility), and EM weights $\alpha_\Omega = 0.2, \omega = 0.8$ for smooth power tracking and bias reduction.

C. LoS Distance Estimation

While the EM–AMP loop uses a single Ω for convergence, the final goal is to estimate the LoS distance d_0, which requires the per-tap profile. This is performed after convergence as follows.

We first select a reliable support $\mathcal{S}$ based on high posterior activity (e.g., $\pi_n > 0.5$). To remove AMP shrinkage bias, we compute a debiased LS estimate $\mathbf{x}_{\mathrm{LS}}$ restricted to $\mathcal{S}$. The refined powers $|\mathbf{x}_{\mathrm{LS},n}|^2$, $n \in \mathcal{S}$, are then fit to the path-loss law. The d_0 estimate solves

$$\hat{d}_0 = \arg\min_{\mathbf{d}_{\min}\leq\mathbf{d_0}\leq\mathbf{d}_{\max}} \sum_{n\in\mathcal{S}} \left[\log\Omega_n(d_0) + \frac{|\mathbf{x}_{\mathrm{LS},n}|^2}{\Omega_n(d_0)}\right], \tag{35}$$

where $\Omega_n(d_0)$ is given by the model in Sec. II-D. The variables $d_{\min}$ and $d_{\max}$ denote the physical search bounds determined by the ISAC system specifications. Specifically, $d_{\min} > 0$ avoids singularity at zero distance and corresponds to the blind zone limit of the receiver, while $d_{\max}$ is determined by the maximum unambiguous range (e.g., $d_{\max} = N\Delta d$) or the sensing power budget. Bounding the search space not only ensures engineering realizability but also limits the computational complexity of the 1D scalar search. This one-dimensional problem is efficiently solved via bounded scalar search, yielding a physically interpretable LoS distance estimate.

D. Computational Complexity

EM-AMP is dominated by $\mathcal{O}(N\log N)$ FFT-based transforms. While the denoiser involves ${}_1F_1(\cdot)$, its element-wise computation adds only $\mathcal{O}(N)$ (e.g., via lookup tables), preserving $\mathcal{O}(N\log N)$ efficiency. This scales better than OMP's $\mathcal{O}(k^3 + kMN)$ updates.

IV. Simulation Results

We now evaluate the proposed EM–AMP framework and its hybrid refinement strategy through Monte Carlo simulations. The experiments are designed to highlight both channel recovery and ranging accuracy.

A. Simulation Setup

A sparse multipath channel is generated under the Bernoulli–Nakagami-m prior, consistent with Sec. II. The channel is probed using a circulant sensing matrix derived from a QPSK pilot sequence. Simulation parameters are summarized in Table I. Performance is evaluated across a signal-to-noise ratio (SNR) range of 0–30 dB in 2 dB increments, with $T = 100$ independent trials per SNR value.

We compare the following estimators:

- **Proposed Hybrid Estimator (`hard_ls`)**: The EM–AMP algorithm followed by LS debiasing on a high-confidence support set (Sec. III-C).
- **Probabilistic AMP Variant (`soft`)**: Uses the raw EM–AMP posterior mean and moments without support hardening.
- **OMP Baseline (`omp_ls`)**: Orthogonal Matching Pursuit with an LS refit on the detected support.

For reference, we also include a heuristic ranging method (`los`) that estimates d_0 from the strongest early tap.

We evaluate performance using Normalized Mean Squared Error (NMSE), support recovery (Precision/Recall), and d_0 relative error. All metrics are standard as defined in [17].

B. Results and Discussion

Representative results are shown in Figs. 2–4. Fig. 2 summarizes the average performance over SNR. OMP-LS achieves slightly lower channel reconstruction NMSE, as it prioritizes residual reduction via greedy search. However, in support recovery, while OMP-LS shows high precision, our EM-AMP framework achieves significantly higher

TABLE I
KEY SIMULATION PARAMETERS

Parameter	Symbol	Value
Channel Length	N	128 taps
Channel Sparsity	k	7 active taps
Nakagami Shape	m	2.0 (fixed)
Path-Loss Exponent	γ	2.5
True LoS Distance	d_0	20.0 m
Distance Resolution	Δd	2.44 m
SNR Range	—	0–30 dB (2 dB step)
Monte Carlo Trials	T	100 per SNR

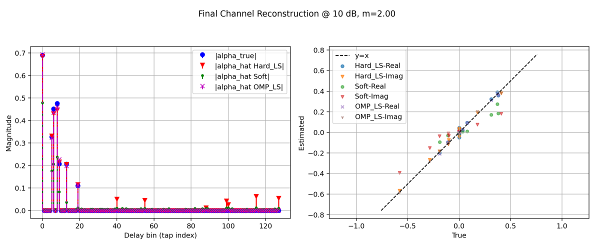

Fig. 1. Example channel reconstruction at SNR = 10 dB.

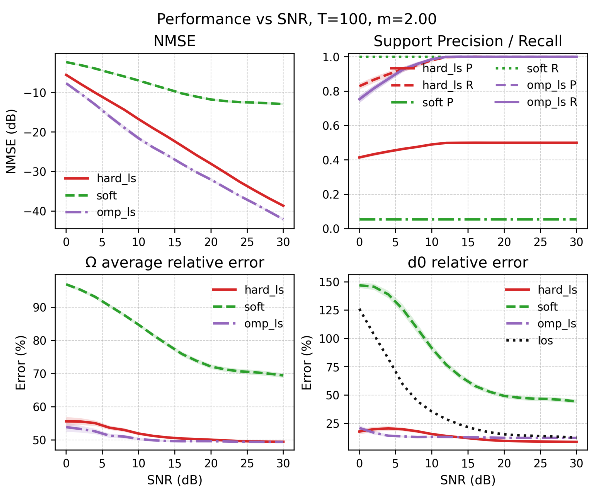

Fig. 2. Performance versus SNR.

recall, which is crucial for robust ranging as it ensures fewer true paths are missed.

Comparing `soft` and `hard_ls` validates that while EM-AMP ensures high support recall, the LS refit is critical to overcome AMP's inherent amplitude shrinkage, leading to the observed significant ranging precision gain (Fig. 4).

As shown in Fig. 3, the OMP-LS estimates show a substantial and persistent bias, clustering around 17.5 m. In contrast, our proposed hard-LS estimates are much closer to the true value of 20 m, demonstrating a reduced ranging bias.

This advantage is more quantifiably shown by the MSE curves in Fig. 4. While OMP-LS performs competitively at very high SNRs, the proposed EM-AMP framework is not only more robust in the low-SNR regime but also achieves a significantly lower MSE for d_0 estimation once the SNR exceeds 15 dB.

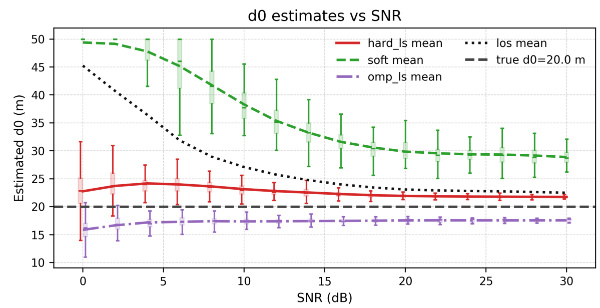

Fig. 3. Estimated d_0 per trial versus SNR.

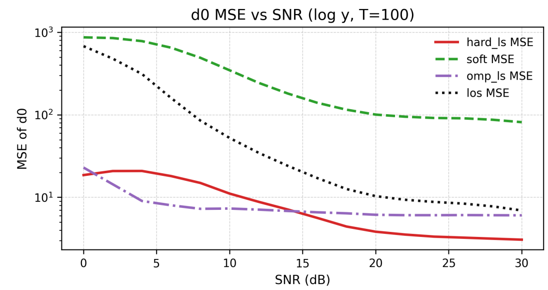

Fig. 4. Mean-squared error of d_0 estimates (log scale).

V. CONCLUSION

We presented an EM–AMP framework for joint sparse channel recovery and ranging in ISAC systems under Nakagami-m fading. The algorithm integrates a closed-form Nakagami-aware denoiser with EM-based parameter learning, enabling the average path power to be estimated directly from the data. A hybrid refinement step further removes the shrinkage bias of AMP, producing sharper power–delay profiles and more accurate line-of-sight distance estimates. Extensive Monte Carlo simulations demonstrated consistent gains over baseline methods, with the proposed approach achieving approximately 3 dB lower ranging MSE at high SNRs. These results confirm that combining a physically grounded fading prior with adaptive parameter learning yields significant benefits for integrated sensing and communication.

In this work, the Nakagami shape parameter m is assumed to be known, which allows us to establish a clear baseline for evaluating the proposed EM–AMP framework under controlled fading conditions. While this assumption is reasonable in scenarios where prior channel statistics are available, extending the framework to jointly estimate m remains an important direction for improving robustness under varying propagation environments.

Future extensions will include joint estimation of the Nakagami shape parameter m, incorporation of Doppler effects for time-varying channels, extensive sensitivity analysis across varying sparsity levels, and validation on more realistic ISAC scenarios. Together, these steps will further enhance the adaptability and practical relevance of the proposed framework.

Acknowledgement: EURECOM's research is partially supported by its industrial members: ORANGE, BMW, SAP, iABG, Norton LifeLock, by the Franco-German project 5G-OPERA (BPI), the French project YACARI (PEPR-5G), the EU H2030 project CONVERGE, and by a Huawei France funded Chair towards Future Wireless Networks.

REFERENCES

[1] F. Liu, Y. Cui, C. Masouros, J. Xu, T. X. Han, Y. C. Eldar, and S. Buzzi, "Integrated Sensing And Communications: Toward Dual-Functional Wireless Networks For 6G And Beyond," *IEEE J. Sel. Areas Commun.*, vol. 40, no. 6, pp. 1728–1767, 2022.

[2] A. Liu, Z. Huang, M. Li, Y. Wan, W. Li, T. X. Han, C. Liu, R. Du, D. K. P. Tan, J. Lu, Y. Shen, F. Colone, and K. Chetty, "A Survey On Fundamental Limits Of Integrated Sensing And Communication," *IEEE Commun. Surv. Tutorials*, vol. 24, no. 2, pp. 994–1034, 2022.

[3] S. Coleri, M. Ergen, A. Puri, A. P. Puri, A. P. Puri, and A. Bahai, "Channel Estimation Techniques Based On Pilot Arrangement In OFDM Systems," *IEEE Trans. Broadcast.*, vol. 48, no. 3, pp. 223–229, 2002.

[4] M. K. Simon and M. Alouini, *Digital Communication Over Fading Channels*, 2nd ed. John Wiley & Sons, 2005.

[5] F. Xiao, Z. Zhao, and D. T. M. Slock, "Multipath Component Power Delay Profile Based Ranging," *IEEE J. Sel. Topics Signal Process.*, vol. 18, no. 5, pp. 950–963, 2024.

[6] T. S. Rappaport, *Wireless Communications: Principles And Practice*, 2nd ed. Prentice Hall, 2002.

[7] J. A. Tropp and A. C. Gilbert, "Signal Recovery From Random Measurements Via Orthogonal Matching Pursuit," *IEEE Trans. Inf. Theory*, vol. 53, no. 12, pp. 4655–4666, 2007.

[8] R. Tibshirani, "Regression Shrinkage And Selection Via The Lasso," *J. R. Stat. Soc. Ser. B*, vol. 58, no. 1, pp. 267–288, 1996.

[9] Y. Chi, L. L. Scharf, A. Pezeshki, and R. Calderbank, "Sensitivity To Basis Mismatch In Compressed Sensing," *IEEE Trans. Signal Process.*, vol. 59, no. 5, pp. 2182–2195, 2011.

[10] D. L. Donoho, A. Maleki, and A. Montanari, "Message-Passing Algorithms For Compressed Sensing," *Proc. Natl. Acad. Sci. U.S.A.*, vol. 106, no. 45, pp. 18 914–18 919, 2009.

[11] M. Bayati and A. Montanari, "The Dynamics Of Message Passing On Dense Graphs, With Applications To Compressed Sensing," *IEEE Trans. Inf. Theory*, vol. 57, no. 2, pp. 764–785, 2011.

[12] S. Rangan, "Generalized Approximate Message Passing For Estimation With Random Linear Mixing," in *Proc. IEEE Int. Symp. Inf. Theory (ISIT)*, 2011, pp. 2168–2172.

[13] S. Rangan, P. Schniter, and A. K. Fletcher, "Vector Approximate Message Passing," *IEEE Trans. Inf. Theory*, vol. 65, no. 10, pp. 6664–6684, 2019.

[14] M. E. Tipping, "Sparse Bayesian Learning And The Relevance Vector Machine," *J. Mach. Learn. Res.*, vol. 1, pp. 211–244, 2001.

[15] D. P. Wipf and B. D. Rao, "Sparse Bayesian Learning For Basis Selection," *IEEE Trans. Signal Process.*, vol. 52, no. 8, pp. 2153–2164, 2004.

[16] A. P. Dempster, N. M. Laird, and D. B. Rubin, "Maximum Likelihood From Incomplete Data Via The EM Algorithm," *J. R. Stat. Soc. Ser. B*, vol. 39, no. 1, pp. 1–38, 1977.

[17] J. P. Vila and P. Schniter, "Expectation-Maximization Gaussian-Mixture Approximate Message Passing," *IEEE Trans. Signal Process.*, vol. 61, no. 19, pp. 4658–4672, 2013.

[18] D. Needell and J. A. Tropp, "CoSaMP: Iterative Signal Recovery From Incomplete And Inaccurate Samples," *Appl. Comput. Harmon. Anal.*, vol. 26, no. 3, pp. 301–321, 2009.

[19] W. U. Bajwa, J. Haupt, A. M. Sayeed, and R. Nowak, "Compressed channel sensing: A new approach to estimating sparse multipath channels," *Proceedings of the IEEE*, vol. 98, no. 6, pp. 1058–1076, 2010.

[20] R. Prasad, *OFDM for wireless communications systems*. Artech House, 2004, vol. 2.

[21] C. Phillips, D. Sicker, and D. Grunwald, "A survey of wireless path loss prediction and coverage mapping methods," *IEEE Communications Surveys & Tutorials*, vol. 15, no. 1, pp. 255–270, 2012.